D. Çanakçı / Hacettepe J. Biol. & Chem., 2021, 49 (3), 185-200

Research Article

Hacettepe Journal of Biology and Chemistry

journal homepage: www.hjbc.hacettepe.edu.tr

Sol-Gel Synthesis And Characterization Of New Inorganic Pigments Containing Oxides of Iron, Aluminum, Strontium and Silicate

Demir, Alüminyum, Stronsiyum ve Silikat Oksitleri İçeren Yeni İnorganik Pigmentlerin Sol-Jel Sentezi ve Karakterizasyonu

Dilek Çanakçı

Vocational School of Technical Sciences, Adıyaman University, Adıyaman, Turkey.

ABSTRACT

A series of inorganic pigments containing iron, aluminum, strontium, and silicate were prepared by the sol-gel method using compounds with different structures and morphologies as starting materials. The synthesis of the compounds was carried out using the modified citrate method. All powders were placed in a muffle furnace and calcined in air at 1100°C for 6 hours. Powder samples containing Fe, Sr, Al and Si oxides were obtained. The structure and chemical composition of the synthesized five inorganic pigments were investigated comparatively by Fourier transform infrared spectroscopy (FTIR), UV-visible spectroscopy (UV-vis), X-ray diffraction (XRD), scanning electron microscopy (SEM), and Energy Distribution X-ray Analysis (EDX).

Key Words

Pigment, SEM, Sol-gel, XRD.

ÖZ

Başlangıç malzemesi olarak farklı yapıları ve morfolojiler olan bileşikler kullanılarak sol-gel yöntemiyle demir, aluminium, stronsiyum ve silisyum içeren bir dizi inorganik pigment hazırlanmıştır. Bileşiklerin sentezi, modifiye edilmiş sitrat metodu kullanılarak gerçekleştirildi. Tüm tozlar bir kül fırınına yerleştirildi ve 1150°C'de 6 saat süreyle havada kalsine edildi, Fe, Sr, Al ve Si'un oksitlerini içeren toz örnekler elde edildi. Sentezlenen beş inorganik pigmentin yapısı, kimyasal bileşimi karşılaştırmalı olarak Fourier dönüşümü kızılötesi spektroskopisi (FTIR), ultraviole-görünür spektroskobisi (UV-vis), X ışını kırınımı (XRD), taramalı elektron mikroskobu (SEM) ve enerji Dağıtıcı X-Ray Analizi(EDX) ile incelenmiştir.

Anahtar Kelimeler

Pigment, SEM, Sol-jel, XRD.

Article History: Received: Feb 19, 2020; Revised: Jan 21, 2021; Accepted: Jan 21, 2021; Available Online: May 5, 2021.

DOI: : https://doi.org/10.15671/hjbc.691065

Correspondence to: D. Çanakçı, Vocational School of Technical Sciences, Adıyaman University, Adıyaman, Turkey.

E-Mail: dcanakci@adiyaman.edu.tr

INTRODUCTION

Pigments are plant- or animal-derived organic and salt- or metal oxide-derived inorganic substances that form colors. They are used in the production of various dyes because of their coloring properties. Unlike dyes, pigments are not soluble in liquids and are held in suspension. Pigments can be metals, metal oxides, salts, or salt mixtures, and in addition to imparting color to paints; they provide properties such as rigidity, corrosion resistance, and opacity. There are various types of inorganic pigments of natural and synthetic origin. Synthetic pigments are synthetic minerals that are obtained by mixing metal oxides or metal-oxide-containing raw materials and being heat-treated at high temperatures (800-1500°C) [1]. Pigments are widely used as coloring agents in paints, coatings, plastics, ceramics, printing inks, cosmetics, and enamels [2, 3]. The most commonly used non-hazardous red pigments are based on iron oxides, because they are non-toxic, have high chemical stability, are commonly found in nature, and have low cost, but the colors shown by iron-red pigments are far less vivid [4–8]. Various studies on the synthesis of new red materials that do not harm the environment continue Red iron oxide (α-Fe_2O_3) pigments have attracted more attention due to their good light fastness, tinting strength, hiding power, durability and low toxicity, and have been widely used in coatings, plastics, ceramics, and other fields. [9,10]. Iron makes up about 6.3% of the Earth's crust; however it is never found in pure form, but instead, combined with other elements, especially oxygen, yielding iron oxides. These iron compounds possess distinct properties such as coloration, resulting from electron transitions between the d (t_{2g} and e_g) orbitals. These colors include yellows and reds, which are responsible for soil colors [11, 12].

In this paper, I document the preparation of new inorganic pigments containing iron, aluminum, strontium, and silicate using sol-gel method and studied their crystal structures, size distributions, morphologies, and chemical compositions. The instrumental techniques used for characterization were Fourier transform infrared spectroscopy (FTIR), UV-visible spectroscopy, X-ray diffraction (XRD), energy dispersive spectroscopy (EDX), and scanning electron microscopy (SEM). Also, the particle sizes of inorganic pigments were determined by X-ray diffractometry.

MATERIALS and METHODS

Materials and Characterization techniques

A series of pigments were synthesized by the sol-gel method. Iron (II) acetate ($Fe(CH_3CO_2)_2$, 95%), Aluminum ammonium sulfate dodecahydrate ($NH_4Al(SO_4)_2.12H_2O$), strontium carbonate ($SrCO_3$, 97%), silicon dioxide (SiO_2, 99.5%), nitric acid (HNO_3, 65%), hydrochloric acid (HCl, 37%), citric acid ($C_6O_8O_7$, 99.5%), and ethylene glycol ($C_2H_6O_2$, 99.0%) were used as starting materials. The FT-IR spectra of the synthesized compounds were recorded on Perkin Elmer Spectrum 100 in KBr pellet over the range of 350-4000 cm^{-1} at room temperature. Absorption spectra were recorded at ambient temperature on a Perkin Elmer Lambda 35 ES UV/Vis Spectrophotometer. The phase composition of the inorganic pigments was detected by X-ray diffraction (Rigaku Smart Lab X-ray diffractometer) with Cu-Ka radiation (1.5405 Å), operated with voltage and current settings of 40 kV and 30 mA, respectively. The morphology of the powders was characterized by a field emission high-resolution scanning electron microscopy (SEM, JSM-6510 Series Scanning Electron Microscope). Also, the same spectroscopy was used to analyze the elemental composition of the sample (EDX).

Method

First, stoichiometric amounts of $Fe(CH_3CO_2)_2$, $NH_4Al(SO_4)_2.12H_2O$, $SrCO_3$, and SiO_2 (5.5 mmol) were stirred at room temperature until they formed a transparent solution in aqua regia (20 mL). To form chelate, a citric acid solution was prepared (22 mmol, 50 mL distilled water), and then ethylene glycol (10 mL) was added into the citric acid solution. The solution of citric acid and ethylene glycol was added into the metal-ion solution, resulting in a completely clear precursor solution. The resulting solution was heated at 80°C and stirred continuously at this temperature for 6 hours. At the end of this period, the water of the solution was removed and an organic gel was formed. Then, it was stored at 70°C in a vacuum oven for 24 hours to ensure complete drying. The dry gel was then transferred into the muffle furnace to be calcined at 1100°C for 3 hours. At the end of the period, the resulting pigments were pulverized and sifted to produce fine and homogeneous powders (Scheme 1).

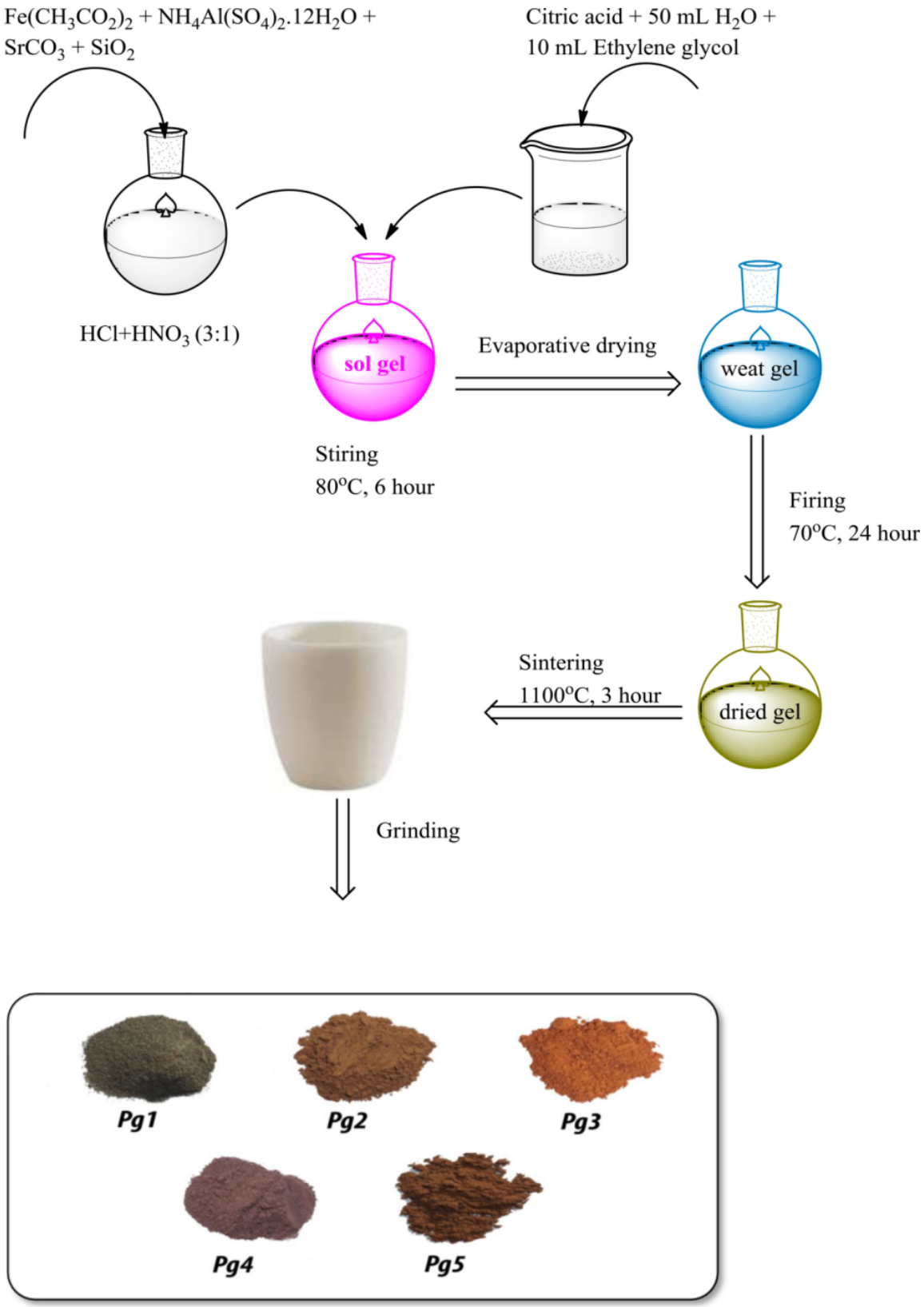

Scheme 1. Preparation of novel inorganic pigments by sol-gel method.

RESULTS and DISCUSSION

X-Ray Diffraction Analysis

The powder XRD patterns of novel pigment compounds showed that sharp peaks were seen between 2θ degrees of 13.60° and 45.23°. Figure 1 shows the powder X-ray diffraction patterns of the inorganic pigment Pg1 ($Sr_4Fe_3Si_2O_4$) calcined at 1100°C. XRD curves indicated that the samples were highly crystalline in calcined air at studied temperature, but the compounds were not single phase. The results of the X-ray diffraction analysis showed that most of the prepared silicium based mixed metal oxides were not single-phase compounds. However, it is not always necessary to obtain a single-phase system in pigmentation, but the synthesis conditions need to be appropriate for industrial use [13-15].

Unlike the other synthesized inorganic pigments, the pigment Pg1 does not have Al metal. The pigment is composed of a mixture of iron, strontium and silicon oxide crystalline phases. The diffraction pattern for Pg1 showed 22 reflections in the range of 17.52°- 43.9°(2Θ). The diffraction peak of SiO_2 was observed for band centered at 2θ= 22.91°, which is the characteristic peak for amorphous SiO_2 (JCPDS No: 1010938). Also, there were peaks corresponding to low quartz SiO_2 at 2θ= 20.86°, 26.47°, 39.47° associated with (100, 101, 102) planes of SiO_2 particles (JCPDS No: 1011172). The XRD pattern of FeO showed a multiphase consisting of FeO and Fe_3O_4, as expected, due to its disproportion. It was found that there existed diffraction peaks with 2θ values of 17.5°, 30.3°, 35.4°, 37.5°, corresponding to the crystal planes of (111), (220), (311), (222) of crystalline iron oxide (JCPDS No: 1011084)[16]. As in FeO, SrO is present in a multiphase consisting of SrO and SrO_2 in the Pg1 pigment. The diffraction peaks appeared at different angles (2θ= 27.2°, 28.0°, 30.6°, 34.2°) corroborated with the JCPDS-7101266 and JCPDS-1010114 values, which can be correlated with the (002), (101), (111), (200), planes of SrO and SrO_2.

Figure 2 shows the XRD patterns of the Pg2 ($Al_2Sr_4Fe_4Si_2O_4$) with different layers of metal oxide. the XRD peaks which could be observed at 13.60°, 18.86°, 24.93°, 27.50°, 30.64°, 33.43°, 34.41°, 35.52°, 40.69°, 44.2°, and 45.2° showed mixed phases of pseudoboehmite (AlO(OH)), boehmite ($Al(OH)_3$) and alumina (Al_2O_3). Clear peaks originating from the reflection of AlO(OH) were observed in the spectra for Pg2. There was a small protuberance at 13.60°, which revealed the existence of AlO(OH) (JCPDS 21-1307). The XRD pattern of the Pg2 sample showed the sharp diffraction peaks at 2θ= 18.86°, 27.50°, and 40.69° corresponding to the (001), (020), (201) diffractions of Bayerite $Al(OH)_3$ (JCPDS 20-0011) [17]. Based on the position of the 24.93°(115), 30.64°(007), 33.43°(222), 34.41°(118), 35.52°(225), and 45.23°(400) peaks corresponds to α-Al_2O_3 and γ-Al_2O_3 phases. Additionally, the weak peak around 44° 2 theta could indicate the formation of γ-Al_2O_3 according to (202) (JCPDS 13-0373)[18]. However, the strong peak at 22.8° could be observed for the existence of SiO_2 as an amorphous phase. Also, the other peaks belongs to SiO_2 occurred at 25.90°(100), 31.53°(102), 30.03°(111), and 40.69°(210) in the XRD. The peaks related to the FeO and Fe_3O_4 were observed at approximately 18.86°(111), 30.64°(220), and 35.52°(311). Also, the diffraction peaks at approximately 27.01°(002), 28.04°(101), 30.03°(111), 34.41°(200) differently observed in the XRD belong to SrO and SrO_2. The highest average crystal size of Pg2 is 100.62 nm.

The XRD pattern of the synthesized Pg3($Al_2Fe_3SiO_3$) pigment is summarized in Figure 3. It is seen that the XRD diffractogram of Pg3 shifted to lower angles compared with the Pg1 and Pg2 and formed fewer peaks. This was due to the absence of strontium oxide in the pigment structure. The characteristic peak corresponding to (020) planes of AlO(OH) (JCPDS Card 01-1283) were observed at 14.05°, while the peak at 41.08° pointed out to the alumina [19-21]. The XRD pattern showed a peak located approximately at 2θ= 21.96°, that suggested an amorphous phase of the SiO_2. Also, the diffraction peaks seen at 24.26°, 33.34°, 35.80° indicated the presence of iron oxide.

The XRD pattern of the Pg4($AlFe_4Sr_4Si_2O_4$) is shown in Figure 4. The results show that the Pg4 formed the 21 diffraction peaks in the range of 17.50-37.78 (2Θ). The diffraction peak broadband centered at 2θ= 22.99°, the characteristic peak for amorphous SiO_2 was not observed. However, the peaks that occurred at 20.99°, 21.96°, 25.91°, 26.48°, 28.06°, 30.04°, and 34.28° indicated the presence of SiO_2. Also, there was a peak corresponding to the residual of unreacted SiO_2 at 2θ= 23.58°, which was associated with (100) planes of SiO_2 particles. According to the XRD pattern result of Pg4, there was no peak indicating AlO(OH) formation, while the peaks proving the presence of $Al(OH)_3$ and Al_2O_3 formed at 24.16°, 30.24°, 33.20°, and 35.49°. The diffraction peaks seen at 17.50°, 24.95°, 30.04°, 33.20°, and 37.78° proved the existence of FeO and Fe_3O_4. The diffraction peaks of SrO and SrO_2 occurred at 27.06 °, 28.06 °, and 30.65 °.

Figure 5 shows the X-ray diffraction pattern of Pg5($AlFe_4Sr_4Si_2O_4$) inorganic pigment. The sharp peaks at 21.93° and 26.44° 2-theta indicate quartz and cristobalite forms of SiO_2 in addition to the peaks at 2θ of 20.93°, 25.86°, and 40.78° corresponding to SiO_2 structure. The XRD peaks which could be observed at 13.58°, 15.17°, 24.66°, 27.52°, 32.46°, 33.44°, 35.61°, 41.59°, 44.21°, and 45.14° belonged to the phases of AlO(OH), $Al(OH)_3$, and Al_2O_3. The peaks related to the FeO and Fe_3O_4 were observed at 24.91°, 30.02°, and 35.03°. In addition, the other peaks of SrO and SrO_2 occurred at 27.01°, 28.04°, 30.63°, and 35.03° in the XRD pattern. The average crystal sizes of the inorganic pigments were calculated using Scherrer's formula (Table 1-5). The highest average crystal size of Pg1, Pg2, Pg3, Pg4, and Pg5 was found to be 186.18 nm, 100.62 nm, 67.68 nm, 133.13 nm, and 97.98 nm, respectively.

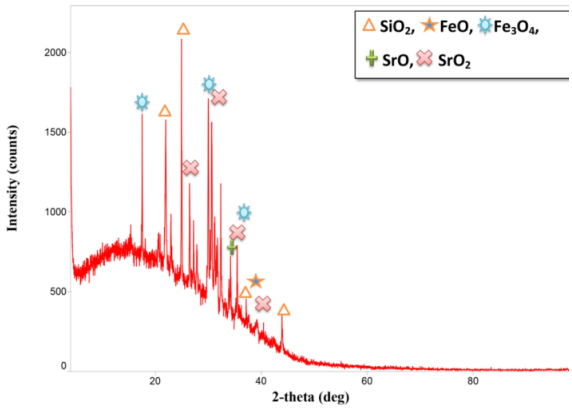

Figure 1. X–ray diffractogram of novel inorganic pigment (Pg1)

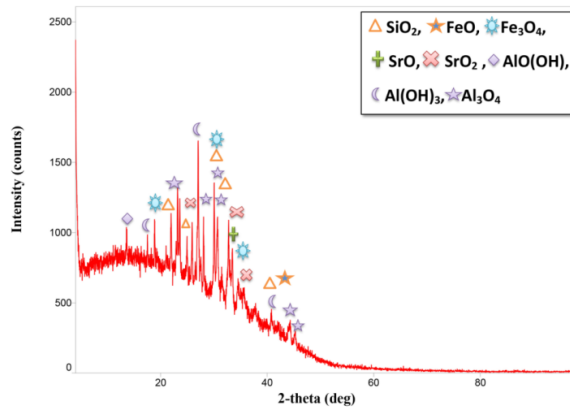

Figure 2. X–ray diffractogram of novel inorganic pigment (Pg2).

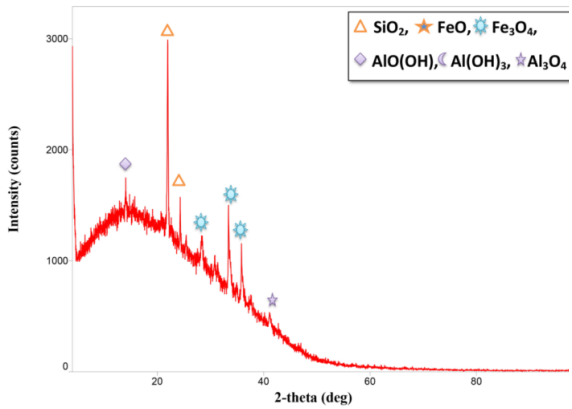

Figure 3. X–ray diffractogram of novel inorganic pigment (Pg3).

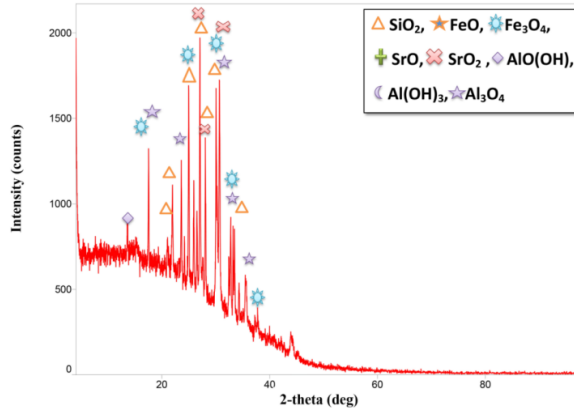

Figure 4. X–ray diffractogram of novel inorganic pigment (Pg4).

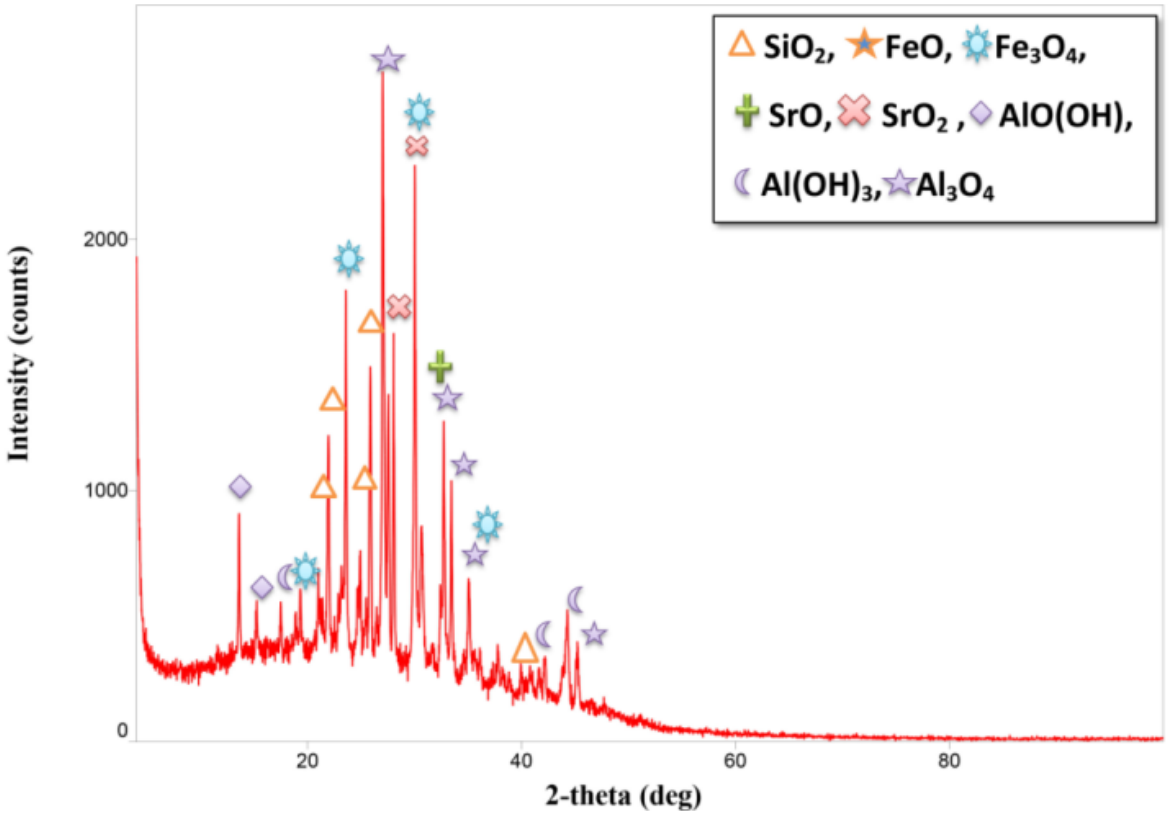

Figure 5. X–ray diffractogram of novel inorganic pigment (Pg5).

Morphology analysis

The surface morphology of the obtained inorganic pigments is presented in Figure 6. SEM micrographs show that each inorganic pigment has its unique structure. The main reason for this is that the metal oxide ratios in their structures are different. The common feature in the SEM micrographs of the pigments is that they show up the formation of a heterogeneous agglomerate mixture of irregular shapes and sizes. The micrographs demonstrate a very similar surface structure of the inorganic pigments (Pg2, Pg3, Pg4, and Pg5), which contain Al in their chemical compositions. According to the SEM micrographs, unlike others, the Pg1 pigment was composed of less aggregated spherical submicron-sized particles and larger layers. Considerably coarsening of more particles can be clearly seen in the SEM micrograph of Pg4. But the phases do not tend to grow into a spherical shape.

The chemical composition of the synthesized inorganic pigment was analyzed by EDX elemental analysis as shown in Figure 7 and Figure 8. The EDX of the synthesized inorganic pigment showed peaks confirming the presence of Al, Fe, Sr, Si, and O elements. Thus, the metal contents of the pigments were confirmed by these results. In the EDX pattern of Pg1, only Fe, Sr, Si, and O peaks were clearly shown and no other peaks were detected. The atomic ratio of Si and O was about 1:2, and the total content of the other elements was about 60.3 wt.%. This means that the strontium oxide and iron oxide shells with high purity have been obtained on the silica microspheres. EDX analysis results of Pg2, Pg3, Pg4, Pg5 showed that the mass percentages of elements other than Si and O were 59.7, 56.4, 57.9, and 50.8 %, respectively. The atomic ratio of Fe:Sr:Al in the Pg1, Pg2, Pg3, Pg4, and Pg5 was about 3:4:0, 4:4:2, 3:0:2, 4:4:1 and 3:4:1, respectively.

Table 1. XRD data of Pg1.

Peak No	İntensity (der)	2θ (der)	d(nm)	FWHM (der)	Cosθ (rad)	FWHM (rad)	D
1	59	17.52	5.057	0.053	0.9883	0.0009	151.60
2	40	20.59	4.311	0.260	0.9838	0.0045	31.042
3	163	21.93	4.048	0.154	0.9817	0.0026	52.525
4	39	22.91	3.878	0.080	0.9800	0.0013	101.28
5	129	24.95	3.565	0.065	0.9763	0.0011	125.12
6	67	26.47	3.364	0.067	0.9734	0.0011	121.76
7	39	27.22	3.273	0.058	0.9718	0.0010	140.87
8	40	27.83	3.203	0.130	0.9706	0.0022	62.933
9	160	30.00	2.975	0.096	0.9658	0.0016	85.640
10	26	30.38	2.939	0.050	0.9650	0.0008	164.57
11	168	30.62	2.917	0.117	0.9644	0.0020	70.371
12	75	31.16	2.867	0.083	0.9632	0.0014	99.327
13	30	31.53	2.835	0.082	0.9623	0.0014	100.63
14	38	31.74	2.813	0.079	0.9618	0.0013	104.50
15	66	32.35	2.764	0.051	0.9603	0.0008	162.13
16	16	33.89	2.642	0.140	0.9565	0.0024	59.298
17	23	34.20	2.619	0.067	0.9557	0.0011	124.01
18	37	35.45	2.529	0.064	0.9524	0.0011	130.26
19	7.3	37.17	2.416	0.045	0.9478	0.0007	186.18
20	7	37,57	2.392	0.180	0.9466	0.0031	46.601
21	16	39,15	2.299	0.380	0.9421	0.0066	22.180
22	32.4	43.91	2.060	0.080	0.9274	0.0013	107.03

2θ: The diffraction angle in degrees, d: interatomic spacing in angstroms, FWHM: full-width at half-maximum, D: Particle size.

Table 2. XRD data of Pg2.

Peak No	İntensity (der)	2θ (der)	d(nm)	FWHM (der)	Cosθ (rad)	FWHM (rad)	D
1	37	13.60	6.505	0.180	0.9929	0.0031	44.429
2	20	18.86	4.700	0.080	0.9864	0.0013	100.62
3	47	21.92	4.051	0.169	0.9817	0.0029	47.862
4	22	22.84	3.890	0.120	0.9801	0.0020	67.513
5	75	23.13	3.840	0.105	0.9796	0.0018	77.198
6	75	23.56	3.772	0.126	0.9789	0.0022	64.381
7	44	24.93	3.568	0.110	0.9764	0.0019	73.935
8	57	25.90	3.436	0.143	0.9745	0.0024	56.982
9	211	27.01	3.297	0.137	0.9723	0.0023	59.613
10	27	27.50	3.240	0.100	0.9713	0.0017	81.756
11	45	28.04	3.179	0.088	0.9701	0.0015	93.012
12	99	30.03	2.972	0.160	0.9658	0.0027	51.388
13	127	30.64	2.915	0.320	0.9644	0.0055	25.730
14	21	31.53	2.835	0.330	0.9623	0.0057	25.005
15	81	32.72	2.735	0.180	0.9594	0.0031	45.979
16	25	32.98	2.714	0.150	0.9588	0.0026	55.212
17	70	33.43	2.678	0.220	0.9577	0.0038	37.689
18	36	34.41	2.604	0.510	0.9552	0.0089	16.300
19	33	35.52	2.525	0.560	0.9523	0.0097	14.890
20	37	40.69	2.215	1.150	0.9375	0.0200	7.3650
21	39	44.28	2.043	0.470	0.9262	0.0082	18.241
22	19	45.23	2.003	0.300	0.9929	0.0052	28.676

2θ: The diffraction angle in degrees, d: interatomic spacing in angstroms, FWHM: full-width at half-maximum, D: Particle size.

Table 3. XRD data of Pg3.

Peak No	İntensity (der)	2θ (der)	d(nm)	FWHM (der)	Cosθ (rad)	FWHM (rad)	D
1	58	14.05	6.297	0.170	0.9924	0.0029	47.065
2	308	21.96	4.043	0.179	0.9816	0.0031	45.191
3	32	24.26	3.666	0.120	0.9776	0.0020	67.687
4	178	33.34	2.684	0.170	0.9579	0.0029	48.764
5	102	35.80	2.505	0.149	0.9515	0.0026	56.010
6	35	41.08	2.195	0.220	0.9363	0.0038	38.548

2θ: The diffraction angle in degrees, d: interatomic spacing in angstroms, FWHM: full-width at half-maximum, D: Particle size.

Table 4. XRD data of Pg4.

Peak No	İntensity (der)	2θ (der)	d(nm)	FWHM (der)	Cosθ (rad)	FWHM (rad)	D
1	55	17.50	5.064	0.089	0.9883	0.0015	90.276
2	38	20.99	4.229	0.200	0.9832	0.0034	40.381
3	77	21.96	4.042	0.179	0.9816	0.0031	45.191
4	80	23.58	3.769	0.092	0.9788	0.0016	88.177
5	16	24.16	3.680	0.061	0.9778	0.0010	133.13
6	134	24.96	3.563	0.123	0.9763	0.0021	66.125
7	65	25.91	3.435	0.123	0.9745	0.0021	66.249
8	42	26.48	3.362	0.126	0.9733	0.0022	64.746
9	190	27.03	3.295	0.109	0.9722	0.0019	74.931
10	27	27.60	3.229	0.160	0.9711	0.0027	51.107
11	95	28.06	3.176	0.094	0.9701	0.0016	87.079
12	175	30.04	2.972	0.110	0.9658	0.0019	74.747
13	59	30.24	2.953	0.094	0.9653	0.0016	87.511
14	242	30.65	2.914	0.146	0.9644	0.0025	56.398
15	33.6	32.45	2.756	0.106	0.9601	0.0018	78.025
16	76	32.76	2.731	0.159	0.9593	0.0027	52.058
17	46	33.20	2.696	0.076	0.9582	0.0013	109.03
18	53	33.47	2.675	0.108	0.9576	0.0018	76.782
19	26	34.28	2.613	0.130	0.9555	0.0022	63.926
20	78	35.49	2.527	0.310	0.9523	0.0054	26.897
21	16	37.78	2.379	0.130	0.9461	0.0022	64.564

2θ: The diffraction angle in degrees, d: interatomic spacing in angstroms, FWHM: full-width at half-maximum, D: Particle size.

Table 5. XRD data of Pg5.

Peak No	İntensity (der)	2θ (der)	d(nm)	FWHM (der)	Cosθ (rad)	FWHM (rad)	D
1	55	17.50	5.064	0.089	0.9929	0.0027	51.596
2	38	20.99	4.229	0.200	0.9911	0.0024	57.230
3	77	21.96	4.042	0.179	0.9832	0.0054	26.052
4	80	23.58	3.769	0.092	0.9816	0.0034	41.062
5	16	24.16	3.680	0.061	0.9788	0.0028	48.869
6	134	24.96	3.563	0.123	0.9763	0.0019	73.940
7	65	25.94	3.435	0.123	0.9745	0.0033	43.114
8	42	26.48	3.362	0.126	0.9735	0.0019	74.155
9	190	27.03	3.295	0.109	0.9723	0.0033	42.536
10	27	27.60	3.229	0.160	0.9712	0.0035	40.475
11	95	28.06	3.176	0.094	0.9701	0.0019	72.436
12	175	30.04	2.972	0.110	0.9657	0.0025	56.318
13	59	30.24	2.953	0.094	0.9643	0.0055	25.733
14	242	30.65	2.914	0.146	0.9602	0.0029	48.646
15	33.6	32.45	2.756	0.106	0.9595	0.0031	46.495
16	76	32.76	2.731	0.159	0.9576	0.0027	51.826
17	46	33.20	2.696	0.076	0.9534	0.0055	26.025

2θ: The diffraction angle in degrees, d: interatomic spacing in angstroms, FWHM: full-width at half-maximum, D: Particle size.

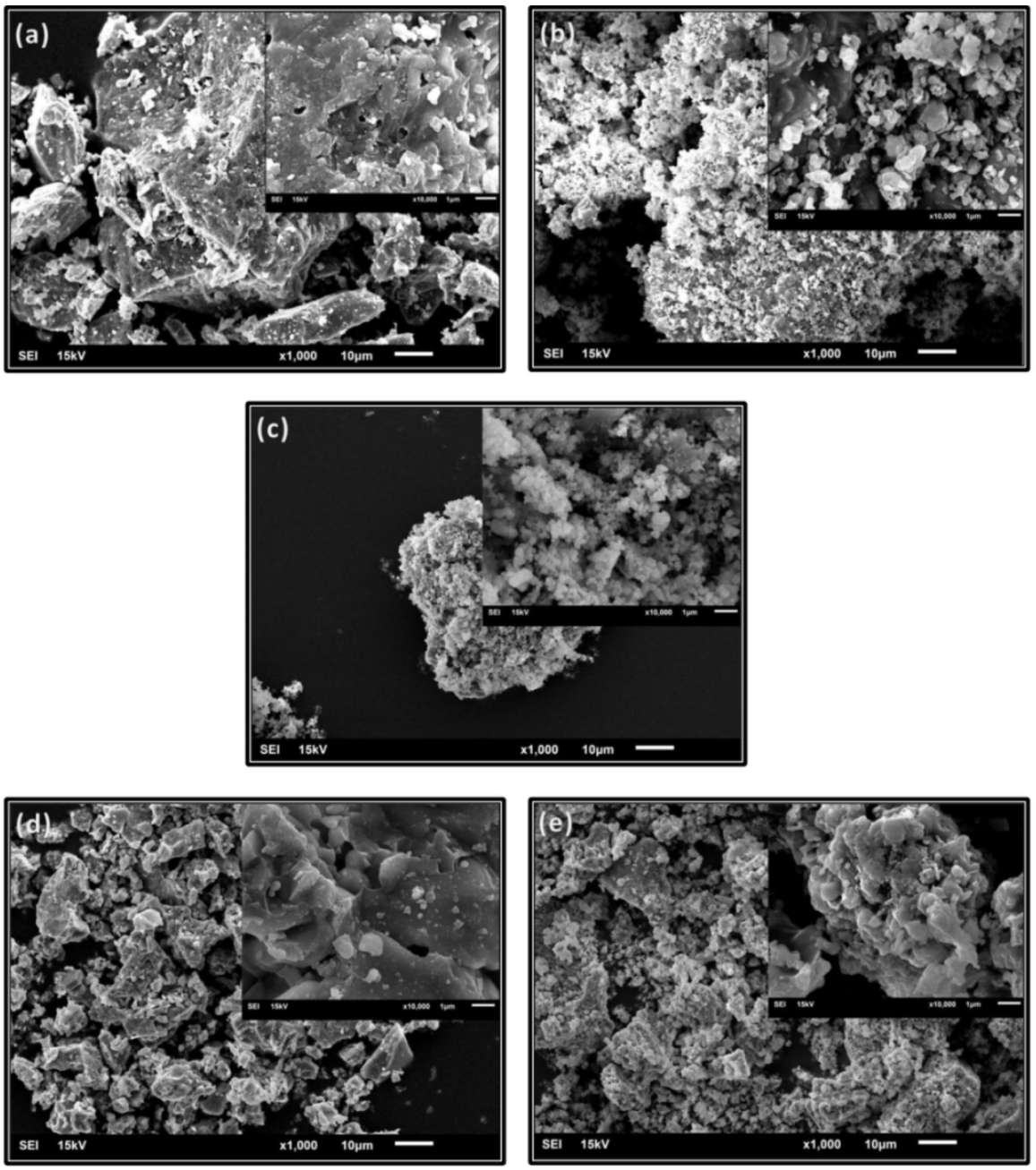

Figure 6. Scanning electron microscopy image of: synthesized pigments : (a) Pg1; (b) Pg2; (c) Pg3; (d) Pg4; (e) Pg5.

FT-IR spectroscopy

To analyze the structure of the prepared inorganic pigments, they were measured using FTIR between 350 cm^{-1} and 4000 cm^{-1} at room temperature. FT-IR spectrum for the Pg1 is shown in Figure 9. FTIR spectrum shows a broadband at 3397 cm^{-1} attributed to O–H stretching from hydroxyl groups and the band at 1603 cm^{-1} is associated with bending H–O–H bond groups of adsorbed H_2O. Broad absorption bands at 1448, 1071, 972, and 926 cm^{-1} agree well with the SiO_2 bond structure. The band at 1448, 1071, and 972 cm^{-1} were assigned respectively to vibrational modes of O–Si–O bending, symmetric stretching of Si–O–Si group and asymmetric stretching of Si–O–Si structural bond of siloxane [22-26]. Besides these three bands, one broad band emerged at 926 cm^{-1} that was usually attributed to the Si–OH stretching vibration. In addition, FTIR spectrum data shows the stretching and bending vibrations of Fe–O bond in the region 359-705 cm^{-1}. According to the literature [27], the wave number 506, 530, 548, 615, and 705 cm^{-1} show the vibration of Fe-O in the Fe_3O_4. Also, the shoulder band at 359 cm^{-1} shows the vibration of Fe–O, as well. In addition, the FTIR spectrum presents a band at 506 cm^{-1}, which correlates with Sr–O stress and confirms SrO formation.

The broadband at 3467 cm^{-1} that is in the Infrared spectrum of pigment Pg2 can be described to the (Al) O–H vibrations of AlOOH and stretching vibration of OH group in the hydroxide structure in absorbed water. The band at 1463 cm^{-1} corresponding to Si–O stretching vibration was observed. The symmetric stretching vibration of the Al–O–H occurred at 1200 and 1132 cm^{-1}. Meanwhile, the peak at 1091 cm^{-1} was also due to the asymmetric stretching vibration of the bond Si–O–Si and γ-alumina due to Al–O vibration mode [28]. The absorption bands in the region 920-993 cm^{-1} are attributed to Si–O stretching vibrations. The broad absorption bands in the range of 399-643 cm^{-1} show the bending vibrations of the Fe–O bond. The absorption bands in the region 920-993 cm^{-1} are attributed to Si–O stretching vibrations. The broad absorption bands in the range of 399-643 cm^{-1} show the bending and stretching vibrations of the Fe–O bond. The Sr–O and Fe–O stretching vibration bands occurred in the form of a wide band in the range of 613-643 cm^{-1}. The weak bands at 399 and 427 cm-1 belonged to Fe–O stretching.

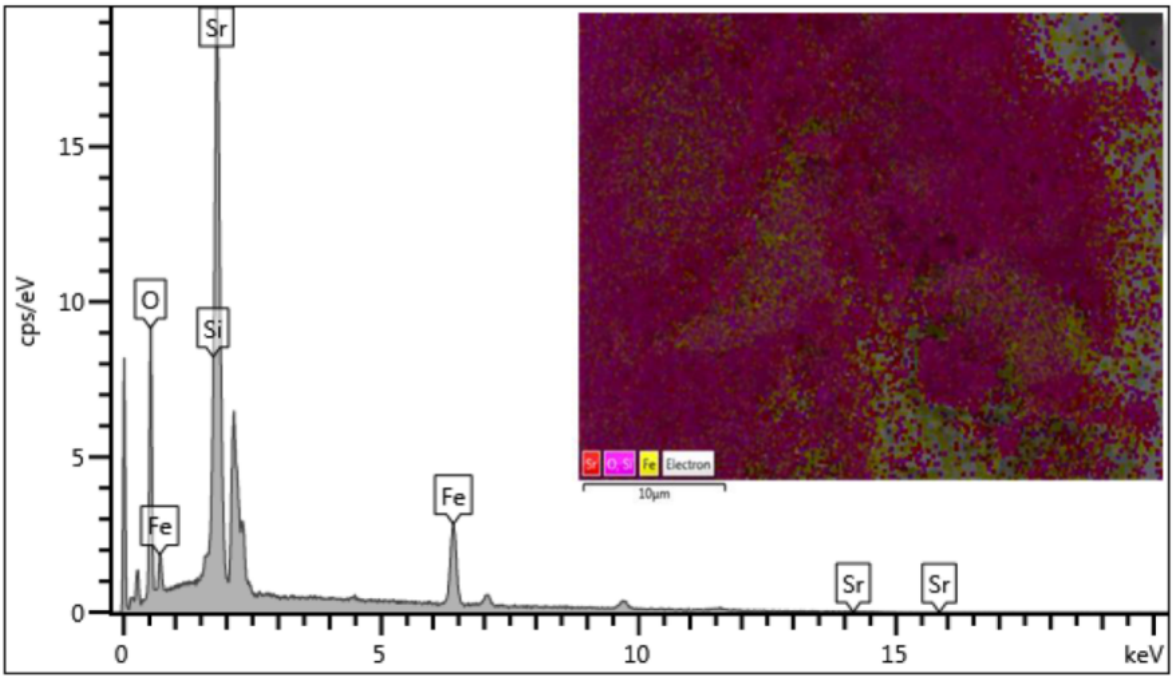

Figure 7. EDX map and spectra of Pg1.

The FT-IR spectrum of the material Pg3 is illustrated in Figure 9. The absorption bands at 3368 cm^{-1} were assigned to the –OH groups of AlOOH. The broad band at 1091 cm^{-1} was related to Al–O and Si–O stretching vibrations. Also, the band at 1463 cm^{-1} corresponding to Si–O stretching vibration was observed, as well. The strong broad bands at 490, 578, 689, and 795 cm^{-1} were assigned respectively to vibrational modes of Si–O bond, to symmetric stretching of Al–O–H bond, and to the bending vibrations of Fe–O bond. The absorption bands at 3390 cm^{-1} and 2691 cm^{-1} that are in the Infrared spectrum of pigment Pg4 can be attributed to the stretching vibration of OH group in the Al–O–H or free H_2O molecules. The Si–O–Si symmetric stretching bands at 1193-1000 cm^{-1} overlapped with the Al–O bonds. The peak in the wave number region of 928-991 cm^{-1} was due to stretching vibrations of Si–O bonds. The bands of low wave numbers of 705, 641, 611, and 550 cm^{-1} observed in the Pg4 pigment spectrum were attributed to the bending vibrations of Al–O bond, the Al–O–Al bond in the gamma phase of alumina generates, and the stretching vibrations of Sr–O stretching vibrations, respectively [29]. The strong band at 435 cm^{-1} and weak shoulder band at 398 cm^{-1} were also due to Fe–O stretching vibrations. The absorption bands showing the presence of the stretching vibration of OH group in the Al–O–H or free H_2O molecules occurred at 3434 and 2084 cm^{-1} in the FTIR spectrum of Pg5. The vibration bands of Al, Si, Sr, and Fe oxides overlapped as in the other inorganic pigments, resulting in the formation of large bands. In the spectrum, the first wide-band formed in the range of 1460-931 cm^{-1} formed as a result of the vibration of Al–O, Si–O and Si–O–Si bonds. Also, the second wide-band observed in the range of 745-447 cm^{-1} was formed by the vibration of Fe–O and Sr–O bonds.

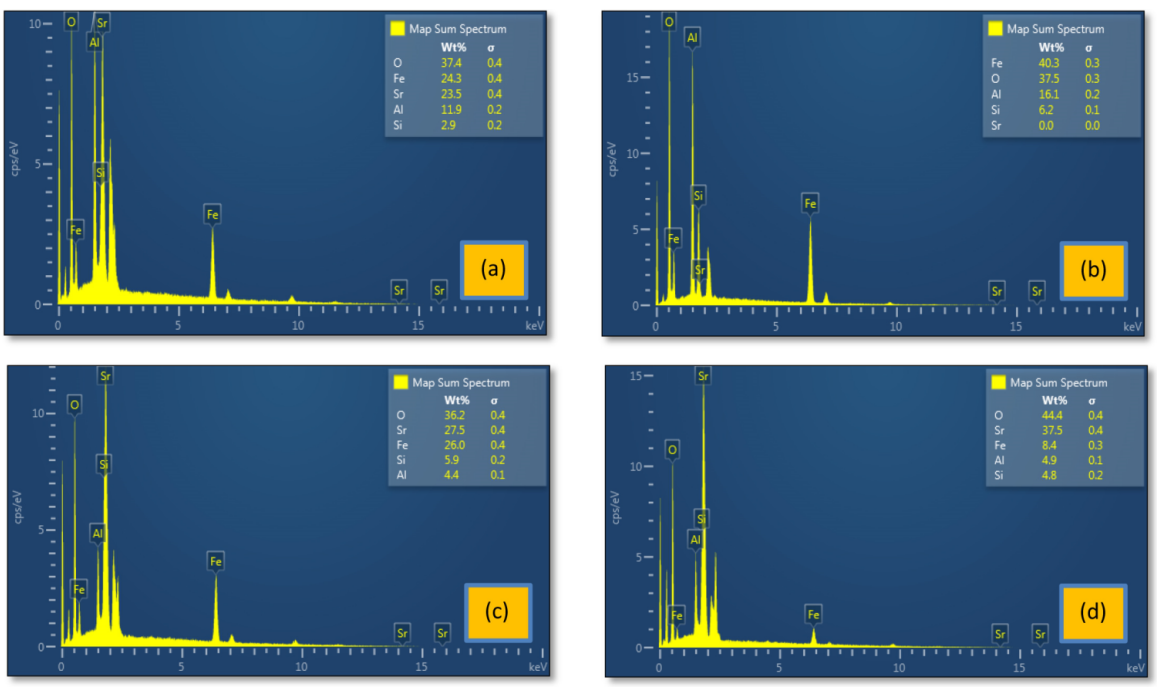

Figure 8. EDX map and spectra of synthesized inorganic pigments: (a) Pg2; (b) Pg3; (c) Pg4; (d) Pg5.

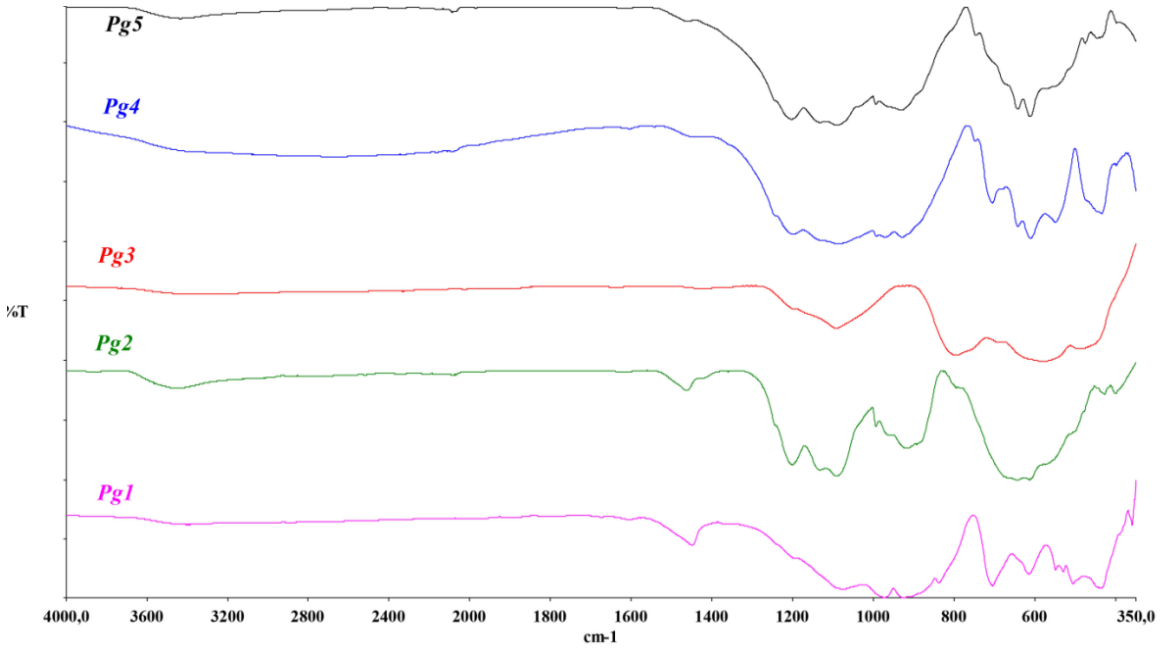

Figure 9. FT-IR spectrum of Pg1, Pg2, Pg3, Pg4 and Pg5.

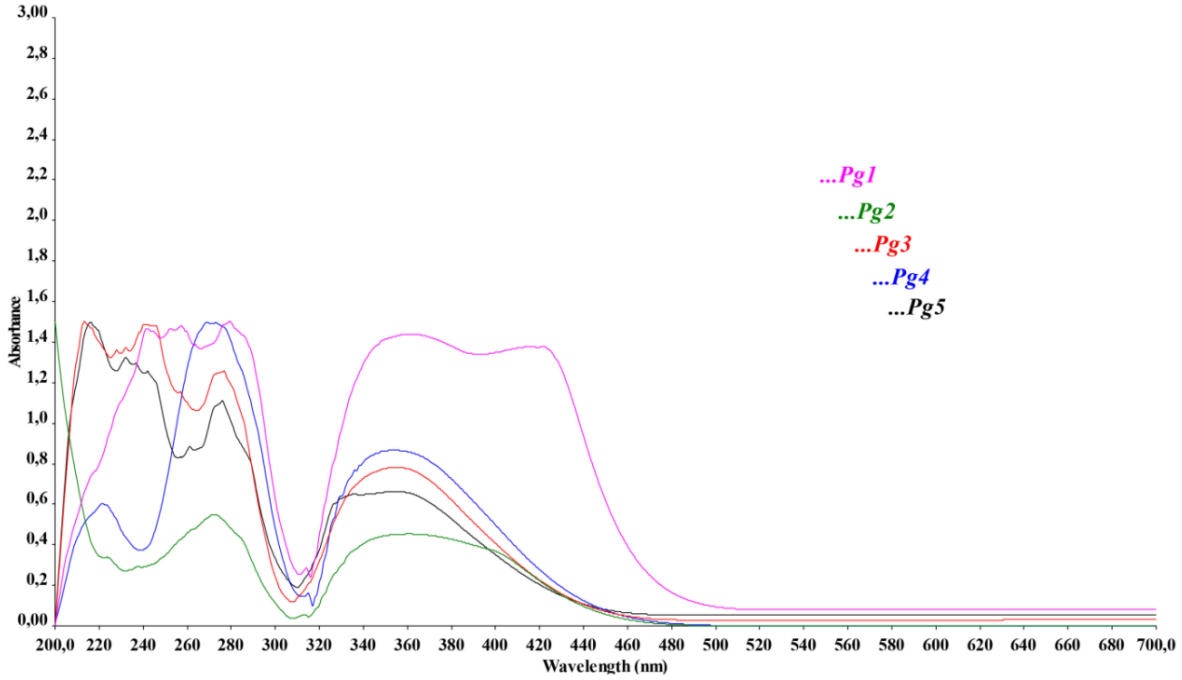

Figure 10. FT-IR spectrum of Pg1, Pg2, Pg3, Pg4 and Pg5.

UV–Visible spectroscopy

The UV-vis spectra of the inorganic pigments are shown in Figure 10. All the synthesized compounds based on metal oxides formed bands in a similar area. Since metals can often interact with many different photons, they form a series of electronic transitions. These transitions can include the metal ion itself or its ligand or ions that bind to the metal ion. As seen in the UV-vis spectra, metals formed a ligand-metal charge transfer and d-d transition. LMCT arises from the transfer of electrons from MO with a ligand-like character to those with a metal-like character. The electron transitions between metals and oxygen provide this transition in inorganic pigments. Pigments other than the pigment Pg1 did not show absorption in the spectral range of 400-700 nm. This result shows that Pg2-Pg5 pigments did not perform d-d transition. Regarding the spectrum of Pg1, it displays its main bands between 241 and 416 nm. The six bands observed in the range of 241-361 nm formed because of the LMCT transition. However, the last band, located at 416 nm, corresponded to the "d-d transition band'', which was assigned to the charge transfer between O^{-2} and Fe^{+3} ion. As a result of charge transfer between oxygen and metal ions in pigments, six absorption bands were formed in the Pg3 spectrum in the range of 213-354 nm, five in the Pg4 spectrum in the range of 221-352 nm, and six in the Pg5 spectrum in the range of 216-353 nm.

Conclusions

In this study, novel inorganic pigments containing containing oxide compounds of iron, aluminum, strontium and silicon metals were synthesized using the sol-gel method. İnorganic pigment structures were confirmed by various spectroscopic analysis. The powder XRD patterns of the new inorganic pigments showed peaks in the expected range. The resulting peaks indicate that the inorganic pigments are not single-phase. This result is an expected condition for inorganic pigments. Due to the different metal oxide ratios in their structures, inorganic pigments have created a unique structure. The obtained sem micrographs show that the pigments form a heterogeneous mixture of agglomerates in irregular shapes and sizes. Also, The EDX results show the Al, Fe, Sr, Si and O peaks, which confirm that the pigments expected metals. IR spectroscopy, one of the spectroscopic methods used to illuminate the structure of inorganic pigments, clearly shows the bands formed as a result of vibrations of metal-metal and metal-oxygen bonds in the structure of pigments.

References

1. E. Taşçı, N. Derin, K.P. Çoşkun, V. Uz, Doğal Zeolitlerin Seramik Pigment Olarak Kullanılabilirliği, AKÜ FEMÜBİD., 14 (2014) 213-218.
2. G. Pfaff, Inorganic pigments, De Gruyter, Berlin, 2017.
3. E.B. Faulkner, R.J. Schwartz, High performance pigments, WileyVCH, Weinheim, 2009.
4. M. Jansen, H.P. Letschert, Inorganic yellow-red pigments without toxic metals, Nature, 404 (2000) 980-982.
5. M.J. Beltran, M.F. Morte, H.B. Mir, E. Cordoncillo, Environmental-friendly red-orange ceramic pigment based on Pr and Fe co-doped $Y_2Zr_2O_7$, J. Eur. Ceram. Soc.., 38 (2017) 2207-2210.
6. M. Llusar, L. Vitásková, P. Šulcová, M. Tena, J. Badenes, G. Monrós, Red ceramic pigments of terbium-doped ceria prepared through classical and non-conventional coprecipitation routes, J. Eur. Ceram. Soc., 30 (2010) 37-52.
7. H. Yuan, J. Zhang, R. Yu, Q. Su, Preparation of ternary rare earth sulfide $La_xCe_{2-x}S_3$ as red pigment, J. Rare. Earths, 31(2013) 327-330.
8. T. Guangyan, W. Wang, D. Wang, Q. Wang, A. Wang, Novel environment friendly inorganic red pigments based on attapulgite, Powder. Technol., 315 (2017) 60-67.
9. H. Hashimoto, K. Higuchi, H. Inada, Y. Okazaki, T. Takaishi, H. Asoh, Welldispersed α-Fe_2O_3 particles for lead-free red overglaze enamels through hydrothermal treatment, ACS Omega, 1 (2016) 9-13.
10. X. Li, C. Wang, Y. Zeng, P. Li, T. Xie, Y. Zhang, Bacteria-assisted preparation of nano alpha-Fe_2O_3 red pigment powders from waste ferrous sulfate, J. Hazard. Mater., 317 (2016) 563-569.
11. J.D. Lee, Química inorganica: Não tão concise, Edgard Blücher Ltda, São Paulo. 1999.
12. J.P. Jolivet, E. Tronc, C. Chaneac, Iron oxides: from molecular clusters to solid. A nice example of chemical versatility, Comptes Rendus. Geosci., 338 (2006) 488-97.
13. Z. Dohnalova, M. Vontoracíkov, P. Sulcova, Characterization of metal oxide-doped lutetium orthoferrite powders from the pigmentary point of view, J. Therm. Anal. Calorim., 113 (2013) 1223-1229.
14. K.J. Sreeram, R. Srinivasan, J.M. Devi, B.U. Nair, T. Ramasami, Cerium molybdenumoxides for environmentally benign pigments, Dyes Pigments, 75 (2007) 687-692.
15. B. Tyliszczak, K.Z. Gaca, A. Sobczak-Kupiec, P. Dulian, Mechanochemical synthesis and investigations of calcium titanate powders and their acrylic dispersions, J. Eur. Ceram. Soc., 34 (2014) 2259-2264.
16. H.S.C. O'Neill, W. Dollase, Crystal structures and cation distributions in simple spinels from powder XRD structural refinements: $MgCr_2O_4$, $ZnCr_2O_4$, Fe_3O_4 and the temperature dependence of the cation distribution in $ZnAl_2O_4$, Phys. Chem. Miner., 20 (1994) 541-555.
17. X. Su, S. Li, J. Li, Effect of potassium sulfate on the low temperature formation of alpha alumina platelets from bayerite, J. Am. Ceram. Soc., 93 (2010) 1904-1908.
18. H.K. Tchakoute, C.H. Rüscher, E. Kamseu J.N.Y. Djobo, C. Leonelli, The influence of gibbsite in kaolin and the formation of berlinite on the properties of metakaolin-phosphate-based geopolymer cements, Mater. Chem. Phys., 199 (2017) 280-288.
19. H.K. Farag, F. Endres, Studies on the synthesis of nano-alumina in airand water stable ionic liquids, J. Mater. Chem., 18 (2008) 442-449.

20. S.C. Shen, Q. Chen, P.S. Chow, G.H. Tan, X.T. Zeng, Z. Wang, R.B.H. Tan, Steam-assisted solid wet-gel synthesis of high quality nanorods of boehmite and alümina, J. Phys. Chem. C, 111 (2007) 700-707.
21. Z. Tang, J. Liang, X. Li, J. Li, H. Guo, Y. Liu, C. Liu, Synthesis of flower-like Boehmite (γ-AlOOH) via a one-step ionic liquid-assisted hydrothermal route, J. Solid State Chem., 202 (2013) 305-314.
22. T. Oh, C.K. Choi, Comparison between sioc thin films fabricated by using plasma enhancechemical vapor deposition and SiO_2 thin films by using fourier transformınfrared spectroscopy, J. Korean Phys. Soc., 56 (2010) 1150-1155.
23. I. Ramalla, R.K . Gupta, K. Bansal, Effect on superhydrophobic surfaces on electrical porcelain insulator, improved technique at polluted areas for longer life and reliability, Inter. J. Engin. Technol., 4 (2015) 509-519.
24. C. Chen, J. Xu, Q. Zhang, H. Ma, H. Miao, L. Zhou, Direct synthesis ofbifunctionalized hexagonal mesoporous silicas and its catalyticperformance for aerobic oxidation of cyclohexane, J. Phys. Chem. C., 113 (2009) 2855-2860.
25. J. Ning, J. Xu, J. Liu, F. Lu, Selective hydrogenation of benzene to cyclohexene over colloidal ruthenium catalyst stabilized by silica, Catal. Lett., 109 (2006) 175-180.
26. M.D. Alba, Z.H. Luan, J. Klinowski, Titanosilicate mesoporous molecular sieve MCM-41: synthesis and characterization, J. Phys. Chem., 100 (1996) 2178-2182.
27. E.M. Lakay, Superparamagnetic iron-oxide based nanoparticles for the separation and recovery of precious metals from solution [Thesis], Matieland (ZA) University of Stellenbosch, 2009.
28. T. Sun, Q. Zhuo, Y. Chen, Z. Wu, Synthesis of boehmite and its effect on flame retardancy of epoxy resin, High Perform. Polym., 27 (2014) 100-104.
29. L.J. Cheng, X. Lan, X. Feng, W.Z. Wen, W. Fei, Effect of hydrothermal treatment on the acidity distribution of γ-Al_2O_3 support, Appl. Surf. Sci., 253 (2006) 766-770.